NANO LETTERS

2007
Vol. 7, No. 9
2747−2752

Electron Shuttle Instability for Nano Electromechanical Mass Sensing

C. Stampfer,* J. Güttinger, C. Roman, A. Jungen, T. Helbling, and C. Hierold

Micro and Nanosystems, ETH Zurich, 8092 Zurich, Switzerland

Received May 25, 2007

ABSTRACT

We discuss the potential use of the electromechanical shuttle instability in suspended nanostructures (e.g., nanotubes or nanowires) for nanomechanical sensing. The tunneling-assisted (shuttle-like) electron transport mechanism is addressed from a mechanical and electromechanical point of view, showing strong dependencies on the fundamental frequency, the mechanical restoring and damping force, and the electromechanical charging of the suspended nanostructure. We propose to use these nonlinear dependencies to sense minute mass (and tension) changes. Therefore, we introduce a conceptual sensing device and investigate its operation in the frame of a simple model system. Finally, we discuss different measurement techniques and report on high sensitivities (e.g., 1 nA/zeptogram (zg), or 1 mV/zg depending on the measurement technique) and potential resolutions in the range of 10 zg (10^{-23} kg).

The ongoing advances in nanotechnology, nanoscience, and nanobiotechnology make ultrafast, high-sensitivity, nanosized sensor systems increasingly important. Nanoelectromechanical systems (NEMS),[1−3] which are not just downscaled microelectromechanical systems (MEMS),[4,5] have been proven to be very promising candidates for such devices.[6] Moreover, NEMS devices may enable novel methods to probe physical processes, chemical reactions, and nanobiological implications at the nanoscale level.

Here, we focus on the high sensitivity detection of a minute mass, which attracts increasing interest in nanotechnology from both an application and fundamental point of view. State-of-the-art minute mass measurement techniques encounter difficulties when (i) investigating dynamic processes, (ii) scaling them down, or (iii) heading toward integration. For example, the time-of-flight mass spectrography[7] can hardly be used to measure reactant mass changes before and after chemical reactions. Moreover, these techniques can hardly be integrated in solid-state M/NEMS. On the other hand, mass detection methods based on the mass-dependent resonant-frequency shift of an oscillator are well suited for fast, highly sensitive detection of single molecules.[8−10] Additionally, these methods can be integrated in solid-state circuits and enable a repeatable, nondestructive technique to measure small mass changes. However, because the resonant frequency shift depends on the relative mass change, the miniaturization of the oscillator toward ultralightweight structures is crucial for highly sensitive mass detection at nanoscale.[9]

Carbon nanotubes,[11,12] one of the most studied nanostructures today, are extremely light, have high aspect ratios, and possess extraordinary mechanical properties, making them a promising material for nanoscaled oscillators[13,14] and nanosensor systems.[15,16] Poncharal et al.[17] showed femtogram mass detection via nanotube cantilevers by using a transmission electron microscope (to track the resonant frequency). Nishio et al.[9] reported zeptogram detection by analyzing secondary electron intensities induced by a focused electron beam of a scanning electron microscope in terms of the oscillation amplitude of a nanotube cantilever. However, these methods (including the optical techniques) share challenging oscillation detection schemes and difficulties for integration in (solid state) micro- or nanoscale systems, which is a major prerequisite for useful future autonomous systems for mass detection at the nanoscale level.

Here, we introduce a transducer concept for mass sensing at the nanoscale based on the tunneling-assisted electron-shuttle instability[18] of a carbon nanotube oscillator.[13,14] The phenomenon of the tunneling-assisted electron shuttle was predicted by Gorelik et al.[19] and has been investigated over the last years.[20] A typical electron-shuttle system includes a movable conducting metal grain clamped in an elastic medium between two metal electrodes. By applying a dc bias, electrons start to tunnel from one electrode to the metal grain, and when exceeding a certain threshold voltage (the system exhibits a bifurcation at some threshold bias), an electromechanical instability occurs, resulting in large-amplitude mechanical oscillations and a shuttle current depending on these oscillations of the grain.

Jonsson et al.[18] showed that such an electromechanical instability can also occur in suspended carbon nanotubes if the bias voltage exceeds a threshold value that depends on the *Q*-factor of the system. In contrast to their work, we focus here on the potential use of the electromechanical instability

* Corresponding author. E-mail: christoph.stampfer@micro.mavt.ethz.ch. Present address: Solid State Physics Laboratory, ETH Zurich, 8093 Zurich, Switzerland.

10.1021/nl0712419 CCC: $37.00
Published on Web 08/25/2007

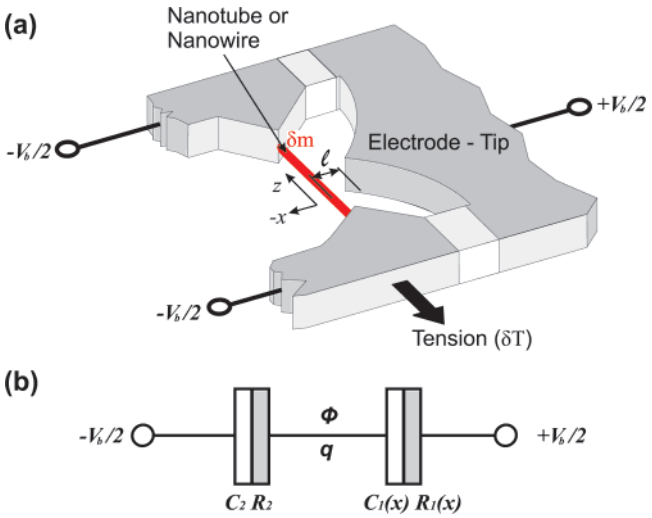

Figure 1. (a) Schematic illustration of the nanoelectromechanical mass sensing device and (b) equivalent circuit of the model system. A suspended nanotube (or nanowire) of length L is clamped by two partially anchored metal electrodes. The nanostructure can be electrostatically displaced by applying a dc-bias voltage V_b at an electrode tip with distance l to the center of the nanostructure. $x(L/2,t)$ measures the deflection of the center of the tube from its equilibrium position. The nanostructure is modeled as a metallic "island" with excess charge q and electrostatic potential ϕ. The electrode-tube contact (and the contact between nanotube and metal electrodes (MEs)) is a tunnel junction characterized by resistance $R_1(x)$ [R_2] and capacitance $C_1(x)$ [C_2].

for nanomechanical sensing. Accordingly, we introduce in the following a model for the proposed sensing device and discuss the influence of several parameters (e.g., coupling strengths, mass variations, mechanical tension) on the shuttle instability. Finally, a few operating modes are proposed and analyzed in terms of typical sensing performance metrics such as, e.g., sensitivity, resolution, and response times.

A schematic illustration of the investigated device is shown in Figure 1a. A metallic carbon nanotube or nanowire[21] of length L is suspended over a trench and clamped by two metal electrodes (e.g., ref 22). The suspended nanostructure can be electrostatically driven by an electrode tip positioned at a distance l of a few nm to the center of the tube. A DC bias voltage V_b is symmetrically applied between the resonator and this electrode, which leads to an electrostatic force F_e attracting the nanostructures. If the redistribution of charge in the nanotube is fast compared to other time constants (e.g., shuttling rates) in the system, the nanotube can be treated as a metallic island with excess charge q and electrostatic potential ϕ. The tip electrode−tube contact (and the nanotube−metal junction) is modeled (Figure 1b) as a tunnel junction characterized by resistance $R_1(x)$ [R_2] and capacitance $C_1(x)$ [C_2].

From a mechanical point of view, the time-dependent bending profile of a suspended doubly clamped nanotube under a driving force distribution $f(x,t)$ is modeled by,[23]

$$EIx_{zzzz} - \left(T + \frac{EA}{2L}\int_0^L x_z^2\,\mathrm{d}z\right)x_{zz} + \rho A x_{tt} = f(x,t) \qquad (1)$$

and $x(0) = x(L) = x_z(0) = x_z(L) = 0$, where A is the cross-sectional area, ρ is the mass density, I the moment of inertia, and E is the Young's modulus. The bracket term in eq 1 describes the stress force in the nanotube, where T is the sum of the residual tensions.[24] Because eq 1 cannot be solved analytically, we make use of the Galerkin discretization procedure[25] to approximate it, leading to a Duffing-type equation of motion. By including a phenomenological damping term $\dot{x}\omega_0/Q$, where Q is the mechanical quality factor, and restricting to the linear regime (neglecting $\mathcal{O}(x^3)$ terms[26]) and the fundamental flexural mode, we obtain

$$\ddot{x}(t) + \frac{\dot{x}(t)\omega_0}{Q} + \omega_0^2 x(t) = \frac{F_e(x,t)}{m_{\mathrm{eff}}},$$
$$\text{where } \omega_0 = \frac{4\pi^2}{L^2}\sqrt{\frac{EI}{3\rho A}\left(1 + \frac{L^2 T}{4\pi^2 EI}\right)} \qquad (2)$$

m_{eff} is the effective mass ($m_{\mathrm{eff}} = k/\omega^2$), and $x(t)$ is a shorthand notation for $x(L/2,t)$, the deflection at the center of the nanotube. The electrostatic force $F_e(x) = -\partial W_e(x)/\partial x$ acts between nanotube and tunnel electrode, where $W_e(x)$ is the free electrostatic energy of the system consisting of two tunneling junctions (Figure 1b). The free energy of this system is given by $W_e(x,q) = (q^2 - 2qC_1(x)V - C_1(x)C_2V^2)/(2C_1(x) + 2C_2)$.[24] To derive the electrostatic force $F_e(x)$, we follow ref 18 and consider a simple plate capacitor model $C_1(x) = C_0(1 - x/l')$, where $l' = l - d/2$.[27] Thus, the electrostatic force is then given by,[28]

$$F_e(x) = -\frac{\partial W_e(x)}{\partial x} = \frac{C_0 l'(C_2^2 V^2 - q^2)}{2[C_0 l' + C_2(l' - x)]^2} \qquad (3)$$

Finally, we assume that the charge q can be treated as a continuum variable. This assumption is justified because the charging energy $E_c = e^2/C_0$ is below $k_B T$ at room temperature.[29] Coulomb blockade is smeared out in these conditions, and a differential equation for the charge q on the nanotube can be written as

$$\frac{\mathrm{d}q}{\mathrm{d}t} = I_2 - I_1 = \frac{Q_2}{C_2}G_2 - \frac{Q_1}{C_1}G_1 = \frac{V}{2}\left(G_- - \frac{C_-}{C_+}G_+\right) - q\frac{G_+}{C_+} \qquad (4)$$

where $G_{1,2} = 1/R_{1,2}$ is the conductance, $R_1(x) = R_0\, e^{-x/\lambda}$ is the nanotube−tip resistance, and $C_\pm(x) = C_1(x) \pm C_2$ [$G_\pm(x) = G_1(x) \pm G_2$] are the sum and difference of the junction capacitances [conductances]. The averaged current can be divided into (i) a tunneling current $\bar{I}_t = T^{-1}\int_{t_0}^{t_0+T} VG_+\,[x(t)]\,\mathrm{d}t$, and (ii) a mechanical shuttle current, $\bar{I}_s$. The average shuttle current is given by the total amount of charge (mechanically) shuttled in one period T, which is approximated by the difference between the maximum and minimum charge on the mechanical shuttle, $\bar{I}_s \approx T^{-1}(q_{\max} - q_{\min})$.

Figure 2 shows steady-state $I-V$ characteristics of the discussed model system. The shuttling current $\bar{I}_s$ and the total current $\bar{I} = \bar{I}_t + \bar{I}_s$ are plotted as a function of the bias voltage

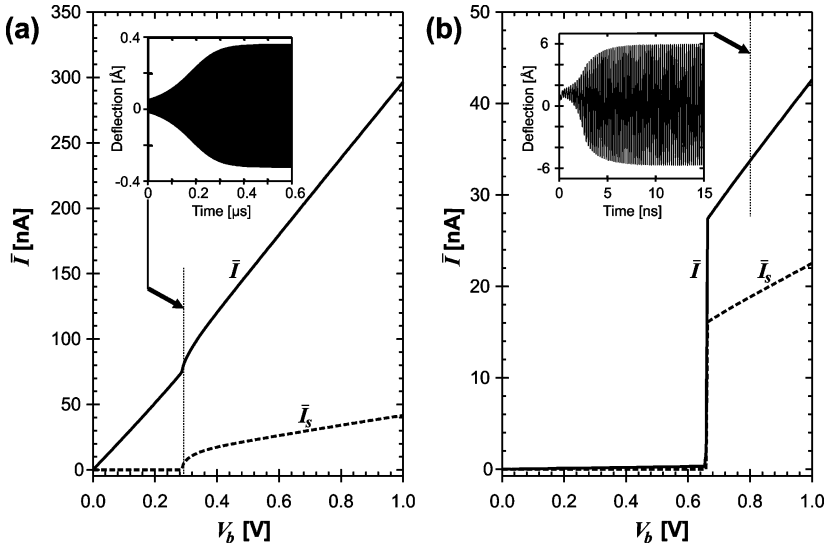

Figure 2. $I-V$ characteristics of the model system corresponding to (a) the soft and (b) the hard transition. For both regimes, the current $\bar{I}$ (solid line) and the purely mechanical shuttle current $\bar{I}_s$ (dashed line) are plotted. The insets depict the transient phenomena for setting up the quasisteady state for two different bias voltages (see dotted line). Please note the different time and amplitude scales for the soft and hard transition.

V_b for two different sets of parameters.[29] Note the qualitative difference between the so-called *soft*-transition (Figure 2a) and the *hard*-transition (Figure 2b) regimes,[18] which, at least technically, only differ in the resistances R_0 and R_2 (soft-transition: $R_0 = R_2 = 2$ MΩ and hard-transition: $R_0 = 2$ GΩ, $R_2 = 20$ MΩ). From an electromechanically charging point of view, however, these two regimes differ significantly because, for the soft-transition regime, small deflections (see inset in Figure 2a)—resulting in a fairly constant $R_1(x)$, $\Delta R_1 \ll R_1$—are sufficient to shift the nanotube potential in order to overcome the damping losses. In contrast, the hard-transition regime requires large deflections (inset in Figure 2b) to provide sufficient charging energy in order to overcome dissipation. Large deflections lead to a strongly nonlinear $R_1(x)$, $\Delta R_1 \sim R_1$, triggering the onset of the highly nonlinear $I-V$ characteristic (Figure 2b).[30] Additionally, the quasilinear and highly nonlinear $I-V$ characteristic significantly affects the transient behavior to tune the electron shuttle (insets in Figure 2). For example, the soft-transition configuration takes approximately 0.4 μs for setting up the quasisteady current for a bias voltage $V_b = 0.29$ V. The inset in Figure 2b shows the much faster, transient phenomena for the hard excitation, where the shuttle current is dominating, $\bar{I}_s > \bar{I}_t$. The quasisteady current (for $V_b = 0.8$ V) is reached in less than 10 ns.

We now focus on the influence of minute mass changes, δm, or applied external tensions, δT, on the electron shuttle. It is assumed (i) that the electrical properties of the nanotube itself are not altered and (ii) that the additional mass δm is homogeneously distributed along the nanotube, which can be replaced by a change in mass density $\delta\rho$. Both, changes in mass and tension are influencing the fundamental resonant frequency of the electron shuttle (eq 2). The frequency shift affects (i) the shuttling rate (increased shuttling current for higher frequencies), (ii) the mechanical force (damping plus restoring) $F_m = m_{eff}\omega_0/Q \cdot \dot{x}(t) + m_{eff}\omega_0^2 \cdot x(t)$, leading to decreased amplitudes for increasing frequencies, and finally, (iii) the charging in dependence of the time constants $\tau_1(x) = R_1(x)C_1(x)$ and $\tau_2 = R_2C_2$. Because the nature of the time constants strongly reflects the soft- or hard-excitation mode, the frequency-dependent charging shows a qualitative difference between the soft- and the hard-transition regimes.

In Figure 3, the current $\bar{I}$ is plotted as function of the tension T for different bias voltages V_b. For the hard transition, the current increases with external stress δT along the nanotube axis until the mechanical restoring force suppresses the amplitude Δx to that point, where the charging energy does not compensate dissipation. This leads to the breakdown of the shuttle current. The threshold tension is a monotonic function of V_b. Less effect is seen for the soft transition, as depicted in Figure 3a. Here, again, the mechanical restoring force dominates over the tension-enhanced charging and leads to the breakdown of the oscillation, resulting in pure tunneling current. The insets of Figure 3 show the time evolution of the mechanical force F_m and the electrical force F_e as a function of the deflection. The restoring force increases for increasing tension at a given deflection and the qualitative difference between soft transition ($\Delta\tau_1 \ll \tau_1$)—quasilinear electrical force F_e (inset in Figure 3a)—and hard transition ($\Delta\tau_1 \sim \tau_1$)—highly nonlinear F_e evolution (inset in Figure 3b)—can be identified. Please note that, in both regimes, for $T = 40EI/L^2$ (no. 2), dissipation is clearly exceeding the driving energy, leading to damped oscillations (e.g., inset in Figure 4a).

The mass sensor characteristic is shown in Figure 4. Because mass changes do only slightly affect the mechanical restoring force because the stiffness $m_{eff}\omega_0^2$ is mass independent, the breakdown of the instability is dominated by the frequency-dependent charging. This has the interesting consequence that the sensor response differs significantly between soft- and hard-transition regimes (Figure 4a,b).

Similar to the current-tension characteristics (Figure 3), the onset of the instable behavior of the hard transition is related to a decreasing frequency (increasing mass), however,

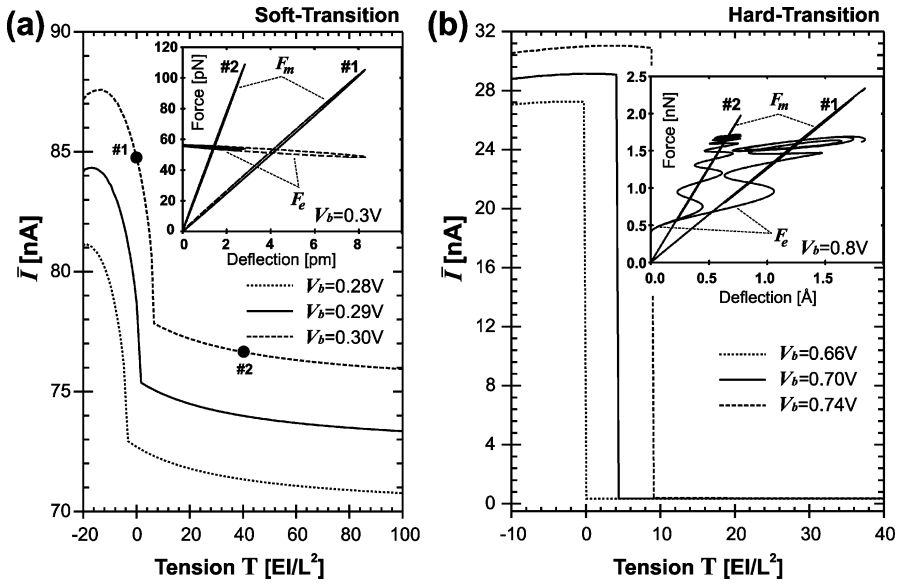

Figure 3. Current vs tension corresponding to (a) the soft and (b) the hard transition for different bias voltages V_b. Please note the different scales for the current, primarily $\bar{I} \approx 0$ for higher tensions in the hard-transition regime. The insets show the time evolution of the mechanical (restoring plus damping) force F_m and the electrostatic force F_e as function of the shuttle deflection for two different tensions T (no. 1: $T = 0$ and no. 2: $T = 40\ EI/L^2$).

it is caused here by the enlarged charging time. Above the threshold value (sufficient mass on the nanotube), the current $\bar{I}$ decreases very slowly due to the decreased shuttling rate. For the soft-transition regime, a completely different $I - \delta m/m_0$ characteristic is observed where a decreasing frequency leads to decreasing current and finally to the shuttle breakdown (see kinks in Figure 4a). This is mainly due to the stronger attraction to the electrostatic equilibrium (dashed line in Figure 4c) of a decelerated electron shuttle. In Figures 4c,d, the time evolution of the electrical force F_e for a certain time interval Δt at a given V_b is shown for different mass densities $\rho_{0,1}$. For both the soft- and hard-transition regime, the decreasing shuttle velocity $\dot{x}(t)$ leads to the instability in the $I - \delta m/m_0$ characteristic (Figure 4a,b). For the hard excitation, the increased charging time, due to the decelerated shuttle (increase in mass; gray curve in Figure 4d), results in an increased F_e and consequently in increasing amplitude Δx and current $\bar{I}$. Within the soft-transition regime, the equilibrium of the potential divider (Figure 1b) is reached for both frequencies $\omega_{0,1}$ at the extremes due to the minor tunnel resistances R_1, R_2. Thus, the difference in mass density only manifests at higher shuttle velocity (arrows in Figure 4c), where the shuttle potential of the decelerated shuttle is closer to the voltage divider equilibrium than the faster shuttle, resulting in less electron shuttling and consequently in damped oscillation. An example of a mass-induced damped oscillation is shown in the inset of Figure 4a. Note that the system has reached the quasistable oscillation state before a relative mass of 8.8% (which corresponds to 3 attograms, 10^{-18}g) has been added and the oscillation has been damped out after $\approx 1.2\ \mu$s. This corresponds to a change in current $\bar{I}$ of $\approx 4.7\%$ (bullets in Figure 4a).

We now turn our attention to the different measurement techniques and perform a brief analysis of each technique in terms of a few standard sensing performance metrics. Four techniques have been identified for the shuttling transducer, three of which can be easily explained with the help of Figures 3,4. The first measurement technique (M1) relies on the monotonic regions of the current-mass (or current-tension) characteristic at constant bias voltage V_b, e.g., $\bar{I}(T)$ for $T \in [-10,9]\ EI/L^2$ at $V_b = 0.74$ V in Figure 3b, or $\bar{I}(\delta m/m_0)$ for $\delta m/m_0 \in [0,0.06]$ at $V_b = 0.2915$ V in Figure 4a. The second measurement technique (M2) involves continuous V_b loop-sweeps while monitoring for a sharp transition (discontinuity) in the output current $\bar{I}$ (either increasing or decreasing). In this case, the value of the bias voltage at the discontinuity, the so-called threshold voltage $V_{b,th}$, yields the mass of (or tension in) the nanotube. The third technique (M3) is a variation of M2 in which the current through the device is kept constant somewhere between the saturated minimum and maximum values (e.g., $\bar{I} = 10$ nA in Figure 4b) by inserting the shuttle in the negative feedback loop of an operational amplifier and forcing the reference current through it. Modifications of the mass (or tension) will directly translate into a variation of the amplifier's output, which corresponds to the threshold bias $V_{b,th}$ for which $\bar{I}$ remains constant at a given mass value. Again, $\delta m/m_0$ (or T) can be derived from $V_{b,th}$. Finally, the fourth measurement technique (M4) exploits a significant difference in the noise levels of the device in the tunneling and shuttling regimes. As for M2, M4 also requires sweeping V_b while monitoring the noise level in $\bar{I}$. M4 in turn admits several variations depending on the frequency band of the monitored noise, discussed below in the context of noise performance of shuttling devices. For practical reasons, we include a discussion of the critical performance parameters of each proposed measurement technique. We focus here on the most important parameters, namely sensitivity, response time, and resolution (limit of detection) and leave aside dynamical

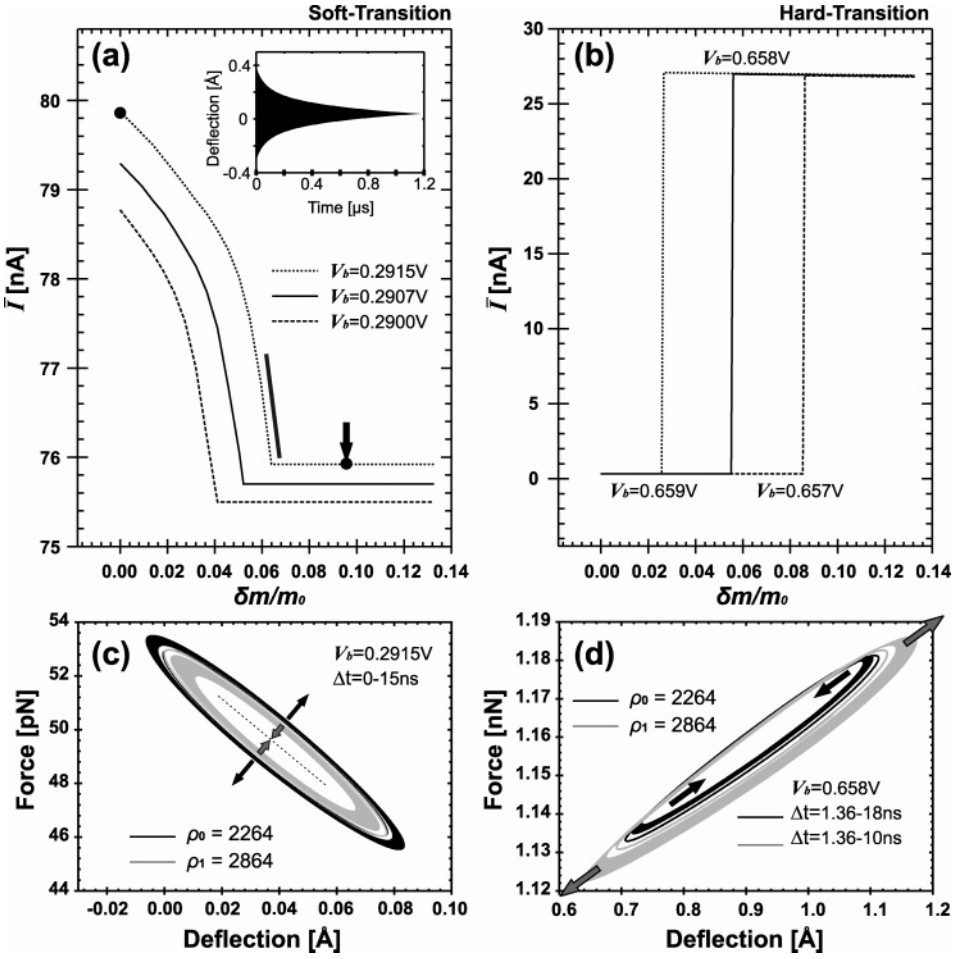

Figure 4. Current vs relative mass change corresponding to (a) the soft and (b) the hard transition for different bias voltages V_b. The inset shows the transient behavior of the shuttle at $V_b = 0.2915$V if 8.8% of m_0 are added to the total mass. The steady state is reached again after 1.2 μs, where the oscillation has died out. The arrow marks this point in the current mass plot. (c,d) Evolution of the electrical force for a time interval Δt as a function of the deflection for two different mass densities ($\rho_{0,1}$) corresponding to (c) the soft and (d) the hard transition. The density is given in units of kg/m^3, and for more information, please see text.

range, linearity, drift, and other parameters. We also restrict the discussion to mass sensing only. The sensitivity of the mode M1 is given by the minimal slope of the $I - \delta m/m_0$ characteristic for any given monotonic segment. For the soft-transition regime (Figure 4a), the calculated sensitivity is around 1 nA/zg for a free nanotube mass m_0 of $\approx$ 34 zg. In the hard-transition regime, the sensitivity is ill-defined because the derivative is singular. We note, however, that in practice, due to finite temperature, the transition will soften, leading to a finite slope and therefore high (but finite) sensitivity. For the remaining measurement modes (M2−4), the sensitivity is approximately the same, and given by $\delta V_{b,th}/\delta m$, yielding the value $\approx$ 1.7 mV/zg for soft-transition and $\approx$ 1.0 mV/zg for hard-transition.

Regardless of the measurement mode, the response time[33] is given by the stabilization of the deflection amplitude (an example of the transient is displayed in the inset of Figure 4a). This stabilization time is generally dependent on the position in the phase space of the system at the moment of the perturbation, the values of the system parameters (e.g., V_b), or, more generally, on the "curvature" of the basin of attraction of the new limit cycle. For the hard-transition regime, we have observed a singularity in the stabilization time as a function of the added mass at the same location as for the $I - \delta m/m_0$ characteristic. In general, we found that the transition time decreases with increasing mass.

The sensing resolution is limited by the noise level quantifiable by the Fano factor, defined as $F = S(\omega)/2e\bar{I}$, where $S(\omega)$ is the power spectral density of the current noise. Because of computational limitations, most of the calculations so far have relied on generalized master equations (e.g., ref 31) in the Coulomb blockade regime at low temperature and small displacements such that the bosonic space could be safely truncated.[32] Therefore, only qualitative conclusions can be transferred to our situation. Although, the Fano factor at zero frequency depends strongly on the restoring force of the nanotube, all studies concur that F differs in the tunneling and shuttling regimes. A second conclusion, evidenced by Isacsson et al.[32] and confirmed later in ref 34, is the presence of a sharp (noise) peak in the Fano factor at the resonant frequency of the nanotube in the shuttling regime only. Therefore, using a low-pass filter or a narrow band-pass around the resonant frequency and measuring the filtered noise, can give information about the shuttling regime. These are the two measurement variants of M4 mentioned before.

Finally, we estimate a potential resolution of the introduced nanotransducer by conservatively assuming that the current noise level $\Delta\bar{I}$ is at the same order of magnitude as the current itself ($\Delta\bar{I} \sim \bar{I}$). Because, for the soft transition (operating in mode M1) the measurable current, $\bar{I}$, is in the range of $\approx$ 10−100 nA, a resolution Δm in the range of approximately 10−100 zg can be estimated. Note that this is of the same order of magnitude as the oscillating carbon nanotube cantilever presented by Nisho et al.,[9] where the oscillation frequency is detected by an electron beam scanning electron microscope.

In conclusion, we have presented a nanoelectromechanical transducer concept to detect minute mass changes (or external tensions) by making use of the electromechanical instability of a nanotube (or nanowire) based electron shuttle. The nonlinear model system has been discussed in detail, and the $I-V$ characteristic for different transport regimes has been revisited. The potential for nanoelectromechanical sensing has been investigated in terms of current-mass (or current-tension) characteristic of the tunneling assisted electron shuttle. We focused in detail on the mechanical implications on the shuttling rate, the mechanical force, and the electromechanical charging. The sensor performance and different measurement techniques have been discussed, and finally, high sensitivities and a resolution in the range of 10−100 zg are estimated, proving the potential to measure minute mass changes. This makes the presented device concept interesting for nanoscaled autonomous mass sensing systems.

Acknowledgment. We thank F. Stampfer, L. Wirtz, R. Grundbacher, and B. Boser for helpful discussions. Financial support by the TH-18/03-1 grant and the Swiss National Science Foundation (20021-108059/1) are gratefully acknowledged.

Note Added after ASAP Publication. There was an error in the exponent that appeared in the abstract in the version published ASAP August 25, 2007; the corrected version was published ASAP August 27, 2007.

References

(1) Craighead, H. G. *Science* **2000**, *290*, 1532−1535.
(2) Ekinci, K. L.; Roukes, M. L. *Rev. Sci. Instrum.* **2005**, *76*, 0611101.
(3) Schwab, K. C.; Roukes, M. L. "Putting Mechanics into Quantum Mechanics", *Physics Today* **2005**, (July), 36.
(4) For general reference on micromachines, see the special issue on Microelectromechanical Systems (MEMS): Technology and Applications, *MRS Bull.* **2001**, *26*, (April).
(5) Hierold, C. *J. Micromech. Microeng.* **2004**, *14*, 1−11.
(6) Roukes, M. L. Nanoelectromechanical Systems. In *Technical Digest of the 2000 Solid-State Sensor and Actuator Workshop*, Hilton Head Island, SC, June 4−8, 2000.
(7) Rose, M. E.; Johnstone, R. A. W. *Mass Spectrometry for Chemists and Biochemists*; Cambridge University Press; Cambridge, U.K., 1982.
(8) Gupta, A.; Akin, D.; Bashir, R. *Appl. Phys. Lett.* **2004**, *84*, 1976.
(9) Nishio, M.; Sawaya, S.; Akita, S.; Nakayama, Y. *Appl. Phys. Lett.* **2005**, *86*, 133111.
(10) Spletzer, M.; Raman, A.; Wu, A. Q.; Xu, X.; Reifenberger, R. *Appl. Phys. Lett.* **2006**, *88*, 254102.
(11) Saito, R.; Dresselhaus, G.; Dresselhaus, M. S. *Physical Properties of Carbon Nanotubes*; Imperial College Press: London, 2001.
(12) Reich, S.; Thomsen, C.; Maultzsch, J. *Carbon Nanotubes*; Wiley-VCH: New York, 2003.
(13) Sazonova, V.; Yaish, Y.; Üstünel, J.; Roundy, D.; Arias, T. A.; McEuen, P. L. *Nature* **2004**, *431*, 284.
(14) Peng, H. B.; Chang, C. W.; Aloni, S.; Yuzvinsky, T. D.; Zettl, A. *Phys. Rev. Lett.* **2006**, *97*, 087203.
(15) Stampfer, C.; Helbling, T.; Obergfell, D.; Schöberle, B.; Tripp, M. K.; Jungen, A.; Roth, S.; Bright, V. M.; Hierold, C. *Nano Lett.* **2006**, *6*, 233−237.
(16) Stampfer, C.; Jungen, A.; Linderman, R.; Obergfell, D.; Roth, S.; Hierold, C. *Nano Lett.* **2006**, *6*, 1449−1453.
(17) Poncharal, P.; Wang, Z. L.; Ugarte, D.; de Heer, W. A. *Science* **1999**, *83*, 1513.
(18) Jonsson, L. M.; Gorelik, L. Y.; Shekter, R. I.; Jonson, M. *Nano Lett.* **2005**, *5*, 1165−1196.
(19) Gorelik, L. Y.; Isacsson, A.; Voinova, M. V.; Kasemo, B.; Shekther, R. I.; Jonson, M. *Phys. Rev. Lett.* **1998**, *80*, 4526.
(20) For a review, please refer to Shekther, R. I.; Gorelik, L. Y.; Galperin, Y.; Isacsson, A.; Jonson, M. *J. Phys. Condens. Matter* **2003**, *15*, R441.
(21) For simplicity, the following description of the device assumes a nanotube being present. However, the nanotube can be simply substitute by a nanowire or any other quasi-one-dimensional metallic nanostructure.
(22) Jungen, A.; Hofmann, S.; Meyer, J. C.; Stampfer, C.; Roth, S.; Robertson, J.; Hierold, C. *J. Micromech. Microeng.* **2007**, *17*, 603−608.
(23) See, e.g., Landau, L. D.; Lifschitz, E. M. *Theory of Elasticity*; Pergamon: Oxford, 1986.
(24) Sapmaz, S.; Blanter, Y. M.; Gurevich, L.; van der Zant, H. S. J. *Phys. Rev. B* **2003**, *67*, 235414.
(25) Nayfeh, A. H.; Mook, D. T. Nonlinear Oscillations. In *Physics and Applied Mathematics*; A Wiley-Interscience Series of Texts, 1st ed.; Monographs and Tracts; John Wiley: New York, 1979.
(26) We numerically validated that the negligence of the $\mathcal{O}(x^3)$ terms originates a deviation in the the current in the range of 10^{-4}%. This, finally, justifies our assumption of not considering this term.
(27) Please be aware that the plate capacitor model is a rather poor approximation. However, other model systems like the capacitance of two spheres, cylinder above plane or point charge next to a plate or sphere have been tested and the x dependency of all these model systems does not show any strong variation. We therefore assume that at the level of the presented model the simple plate capacitor model holds to describe the electrostatic force F_e.
(28) Note that this equation completely agrees with ref 18, where the following expression is used for the electrostatic force $F_e(x) = F_0(C_2V + q)^2/(1 - \alpha x)^2$. By setting $F_0 = C_0/l(C_0 + C_2)$ and $\alpha = C_2/l(C_0 + C_2)$, we find eq 3.
(29) Used parameters: $L = 200$ nm, $r_o = 5$ nm, $r_i = 1$ nm, $\rho = 2264$ kg/m^3, $l = 6$ nm, $\lambda = 0.5$ Å, $E = 1$ TPa, $Q = 50$, $C_0 = 5 \times 10^{-18}$ F, and $C_2 = 5 \times 10^{-18}F$. The charging energy is close to 16 meV, which is below 25 meV ($= k_BT$).
(30) Here, the time or deflection dependency of capacitance $C_1(x)$ is assumed to be much weaker than the relative influence on $R_1(x)$.
(31) Flindt, C.; Novotny, B.; Jauho, A. P. *Physica E* **2005**, *29*, 411−418.
(32) Isacsson, A.; Nord, T. *Europhys. Lett.* **2004**, *66*, 708−714.
(33) The response time is the time duration necessary for the system to get to 90% of the steady-state value.
(34) Utami, D. W.; Goan, H. S.; Holmes, C. A.; Milburn, G. J. *Phys. Rev. B* **2006**, *74*, 014303.

NL0712419